1. 疾患概念

脳梗塞はNIDDSの分類に基づき，臨床病型として①アテローム血栓性脳梗塞，②心原性脳塞栓症，③ラクナ梗塞，④その他の脳梗塞に分類される．具体的な診断指針としては，TOASTの基準[1]により，アテローム血栓性脳梗塞では，大脳皮質症状，脳幹，あるいは小脳症状を呈し，その病巣の責任血管にアテローム硬化による50%以上の狭窄あるいは閉塞を認め，梗塞巣は1.5 cm以上の大きさを呈する．心原性脳塞栓症とは心房細動をはじめとする心疾患があり，そこからの血栓が栓子となって塞栓性に血管を閉塞させて生じる脳梗塞である．ラクナ梗塞は典型的にはFisherの提唱したラクナ症候群を呈し，大脳皮質症状を伴わず，画像で脳幹あるいは皮質下白質に1.5 cm未満の病巣が描出される．このように，臨床病型まで含めた脳梗塞の診断には，梗塞巣の診断のみならず，主幹動脈病変の把握が必要である．脳梗塞は欧米では発症3時間以内の超急性期であればtPAによる血栓溶解療法の適応が認められており（本邦では治験中），いかに早期に診断するかが重要となっている．本邦においては様々な抗血栓療法が可能であり，的確な治療のためには臨床病型を早期に診断することが必要である．

2. 読影のポイント

頭部CTによって脳梗塞が明瞭に描出されるには一般には24時間以上必要であるが，発症数時間以内でも島皮質の不明瞭化・皮質髄質境界の不明瞭化・梗塞巣がやや低吸収域・脳溝の狭小化・脳室の軽度圧排・中大脳動脈主幹部に索状の高吸収陰影（hyperdense MCA sign）といったearly CT signが認められる場合がある．しかし，微妙な変化であり，診断が難しい場合が多い．これに対して，MRによる拡散強調画像では，発症30分後には梗塞となった部分では拡散の低下が起こり，梗塞巣の描出が可能と考えられる．ただし，拡散強調画像で描出されるのは虚血中心部の組織壊死を起こした部分であり，梗塞巣周囲に広がるpenumbraとよばれる脳虚血領域が広範である場合には，時間経過とともに脳梗塞巣は徐々に広がる[2]．超早期の拡散強調画像で臨床症状と一致しない場合には拡散強調画像で描出された梗塞巣が拡大する可能性があることには注意する必要がある．また，脳幹梗塞は超急性期には拡散強調画像で病巣が描出されにくい場合がある[3]．このように超急性期の診断にMRは有用であるとともに，CTと比較すると，一般に脳表および脳幹・小脳の梗塞巣の描出に優れている特徴がある．さらに，MRアンギオを加えることで主幹動脈，特に頭蓋内の動脈硬化病変が描出できる点が臨床上は重要である．

3. 診断の手順

急性に発症した局所神経症状を認めた場合には脳血管障害である可能性が高い．血栓溶解療法の適応を念頭に置き，できるだけ早く脳出血を除外する必要がある．一般に緊急で検査しやすいのはCTであり，これにより脳出血・くも膜下出血を除外する．脳梗塞の臨床病型を診断するためには，MR拡散強調画像による病巣の描出，頭蓋内の主幹動脈病変の診断のためにMRアンギオを行う．頭蓋外の内頸動脈起始部病変に対してはMRアンギオや頸部超音波検査法により血管病変をとらえ，心電図，胸部X線，臨床所見から心原性塞栓の塞栓源となる心疾患の把握が行えれば，臨床病型の確定診断が可能となる．

文献

1) Adams HP Jr, Bendixen BH, Kappelle LJ, Biller J, Love BB, Gordon DL, et al. Classification of subtype of acute ischemic stroke. Definitions for use in a multicenter clinical trial. TOAST. Trial of Org 10172 in Acute Stroke Treatment. Stroke 1993; 24(1): 35-41.
2) 星野晴彦，高木　誠．脳卒中への初期対応はなぜ必要か．モダンフィジシャン 2001; 21(7): 894-7.
3) Oppenheim C, Stanescu R, Dormont D, Crozier S, Marro B, Samson Y, et al. False-negative diffusion-weighted MR findings in acute ischemic stroke. AJNR Am J Neuroradiol 2000; 21(8): 1434-40.

特集／脳卒中 — 診断と治療のめざましい進歩

脳卒中診断の進歩とその応用

脳梗塞急性期診断に欠かせないDiffusion MRI

星野晴彦　高木誠

CTの出現は，脳出血を発症直後に診断できることから，脳卒中診療の大きな進歩であった。しかし，脳梗塞巣は発症当日には描出されないことが多く，発症翌日にCTを再検査して初めて梗塞巣の大きさと位置が確認されることが多かった。その後にMRが出現し，CTで診断ができなかった後頭蓋窩や脳表の小さい脳梗塞の診断が可能となったが，Spin Echo法によるT2強調画像やproton密度画像は，脳卒中の超急性期の描出能力としては，CTよりもやや鋭敏ではあるが，まだまだ不十分であった。しかし，MRの撮像法と機器の進歩によるDiffusion MRの出現により，脳梗塞患者で来院時にほとんどの症例で梗塞巣の描出が可能となり，超急性期脳梗塞の診療に飛躍的な進歩をもたらすことになった。今回はCTで診断可能な脳出血，くも膜下出血は除いて，脳梗塞に絞って解説していくことにする。

Ⅰ．Diffusion MRとは何を表しているのか？

現在，臨床で用いられているMRは水素原子の状態を画像化している。水素原子は，生体中では，水分子の中に最も多く存在することから，MRは生体の水の状態を画像化していることになる。水分子は，ブラウン運動によって常に動いており，その水分子の微細な運動状態を画像化することが，Diffusion MRである。

水の拡散状態を画像化することは，以前よりその臨床的な有用性が有望視されていたが，撮影に長時間を要することから臨床応用が遅れていた。撮像法としてEcho Planar法による超高速撮影が可能となって，一般の臨床で用いることができるようになった[1]。撮影の原理としては，ブラウン運動による拡散が増すと，スピンの拡散が起こるために見かけ上T2*の信号強度が低下することを利用して画像化する。拡散は3次元で起こるため，撮影は3次元の平均（x，y，z軸方向にそれぞれ撮影してその値の平方和の平均）を用いて表現するのが一般的である。また，実際に得られる画像は拡散強調画像であって，拡散だけの画像ではないため，特に，横緩和時間T2の影響を受けることに，読影上，注意が必要となる。拡散強調画像での信号強度の異常が拡散の異常であるのか横緩和時間の異常によるものかを検討するには，T2強調画像との比較と，拡散係数の画像(Apparent Diffusion Coefficient map：ADC map）を検討する必要がある（図1）。

東京都済生会中央病院神経内科

Ⅱ．脳梗塞における拡散変化の病態

脳が梗塞になるとその超早期から拡散状態が変化するが，その病態は，脳梗塞の最初の時期であるcytotoxic edemaの時期に拡散係数が低下するためと考えられている。これは，脳虚血の結果，脳組織が細胞の代謝機能を保てないレベルまで脳血流が低下すると，細胞膜のNa^+-K^+-ATPaseが失活し，細胞外から細胞内への水の移動が起こり細胞内の拡散係数の低い水が増え，同時に細胞外領域の狭小化により拡散係数の高かった水が減少することによって拡散係数の低下が起こるためと考えられている。この拡散係数（ADC）の低下は，24時間後頃に最低となり[2]，その後最初の3～4日以内は低下しているが，5～10日になるとほぼ正常値に戻ってくる[1]。

拡散強調画像では，梗塞巣は当初はADCの低下に伴い，高信号な病巣として描出されるが，その後にT2緩和時間の低下が生じて信号強度が高

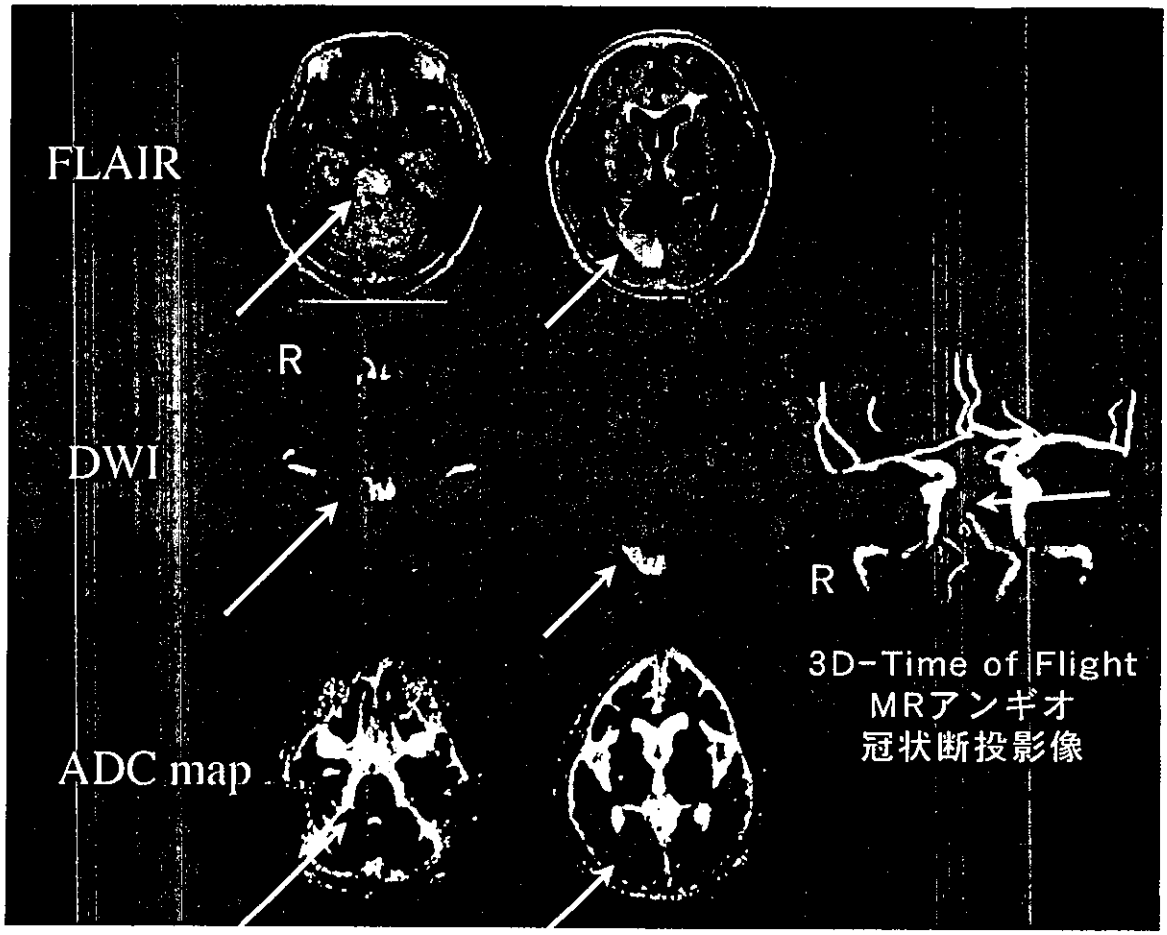

MR アンギオ(MRA)で脳底動脈が閉塞し，FLAIR で右後頭葉と橋に梗塞巣を認める。両梗塞巣とも拡散強調画像(DWI)でも高信号であるが，ADC map では，橋は低信号であり，数日以内の梗塞であることがわかるが，後頭葉の病巣はほぼ等信号となっており，梗塞巣の発症時期が異なることがわかる（経過からは後頭葉症状は７日前の発症であった)。

図　1　血栓性脳底動脈閉塞症例

くなるため，ADC が正常化しても T2 信号強度によって病巣は拡散強調画像ではしばらくの間は高信号として描出されることになる。脳梗塞巣の拡散強調画像での高信号の変化を定量的に調べた報告によると，拡散強調画像の信号が最も高くなるのは約40時間後であり，高信号が消失するのは平均57日目であった。ADC の値が正常な対側と同じになるのは発症後9.8日であり，ADC の信号が最も強くなるのは28.2時間後であった[3]。拡散強調画像における信号強度に対する ADC と T2 の影響をまとめると，発症後３日目までは，ADC の低下によって信号強度が上がっているが，３日目以降は T2 による信号強度の変化の影響が強くなり（T2 shine through)，10日以降は ADC の低下は正常化してむしろ上昇するため，ADC の変化は信号を下げる方向に働くようになるが，T2 の変化の方が優勢なために高信号のままで推移するということになる（図２)。ただし，これらの

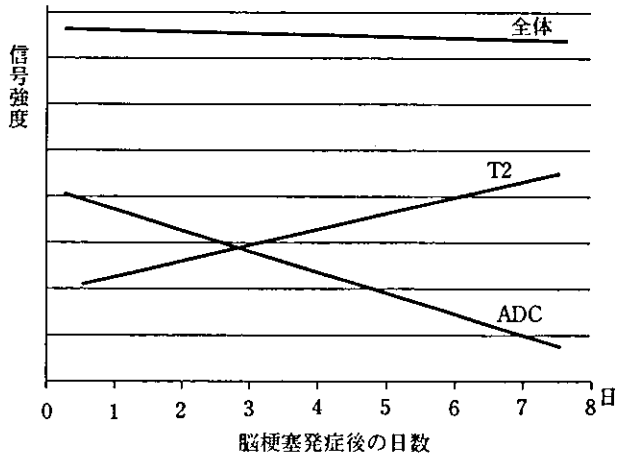

T2 と ADC の経時的変化と全体の信号に与える影響。発症３日までは ADC の変化によって高信号となっているが，３日目以降は T2 の変化によって信号強度が増す（T2 shine through)。

図　2　拡散強調画像における信号強度の経時的変化

定量的な変化は撮影のパラメーターが異なると変化することにも注意が必要である。拡散強調画像

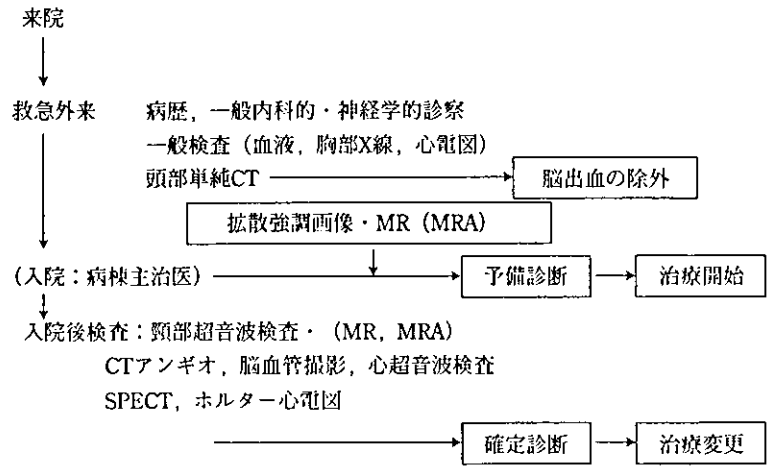

救急外来でCTにより脳出血が除外され，脳梗塞と診断された段階で初期診療が開始され，種々の検査後に確定診断，治療の見直しが行われることが多かった。拡散強調画像をはじめとしたmutimodal MRの出現により，救急外来レベルで臨床病型まで含めた梗塞の病態の把握が容易となり，血栓溶解を含めた初期治療から最も有効な抗血栓療法が行えるようになった。

図 3　脳梗塞患者の診療の流れ

を撮影する際のb値を通常の1,000よりも大きくすると，ADCの低下による信号強度の変化を強く反映した画像が得られる。b値を3,000にするとADCの低下による信号強度はb＝1,000の時の2倍以上の信号強度が得られ，信号強度がADCの変化からT2の変化が優勢となるT2 shine throughとなるのは，3日目から6日目になると計算されている[4]。

Ⅲ．拡散強調画像の脳卒中診療における位置づけ

拡散強調画像は拡散の低下を画像上で描出できる唯一の方法であり[5]，そのためにCTよりも正確に早く梗塞巣を描出することが可能である[6]。発症3時間以内のtPAによる血栓溶解療法の有用性が示されてから，脳梗塞はBrain Attackとして1分でも早く治療を開始すべき緊急疾患であり，そのためには発症直後より脳虚血の病態を診断する必要がある。拡散強調画像は，脳梗塞発症直後より病巣の描出が可能であるということで，心筋梗塞における心電図と同じような臨床的な意味を持っていることになる[7]。つまり，心筋梗塞において心電図が発症直後より異常を示すように，拡散強調画像は脳梗塞巣を発症直後より描出できるという点で，脳梗塞診療においては画期的な診断法といえるわけである。

脳梗塞診療における拡散強調画像の位置づけを図3に示した。発症直後に来院した脳卒中患者の場合には，まずCTによって脳出血・くも膜下出血や脳卒中以外の疾患（脳腫瘍や慢性硬膜下血腫など）が除外されると，脳梗塞と診断され初期治療が開始され，その後にCTの再検やMRによって脳梗塞巣の確認と梗塞の臨床病型の診断がなされるのが，それまでのプロセスであった。拡散強調画像の出現により，梗塞の確認が極く早期に行えるようになったことになる。さらに，MRの種々のパラメーターを用いた画像解析により，CTを使うことなく，出血性病変の診断も可能と考えられつつあり，拡散強調画像とMRアンギオ，灌流画像といったいくつかの撮影方法を用いるmultimodal MRにより，予備診断の段階で梗塞の病態が正確に診断できるようになり，血栓溶解療法を含めた臨床病型に応じた有効な抗血栓療法が行えるようになる（図4）。

また，拡散強調画像では新しい病巣の確認が容易であり，臨床的に無症状な病巣が描出される場合も多く，脳梗塞の病態把握と臨床病型診断に極めて有用である（図5）。

Ⅳ．脳梗塞発症直後では拡散強調画像の異常領域は経時的に拡大する場合が多い

脳梗塞の病態を考えた場合，脳虚血の強い虚血の中心部位は，数分間で細胞死のレベルの虚血となり，その結果，拡散強調画像で異常領域として描出できるようになる。しかし，その中心部を取

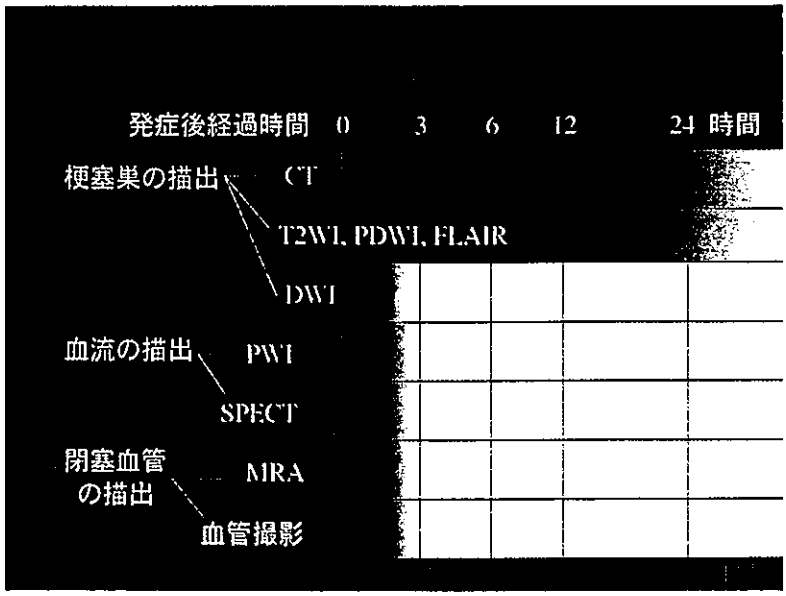

CT および T2WI・PDWI（プロトン密度画像）や FLAIR に比べて DWI（拡散強調画像）は極めて早期に梗塞巣の描出を可能とした。血流検査および閉塞血管の描出が MR の撮影法の選択によって可能であり，MR 装置による muldimodal MR がこれらの病態把握に必要な画像をすべて撮影できる。PWI：灌流画像，MRA：MR アンギオ

図　4　　脳梗塞急性期の各画像診断で陽性となる時期

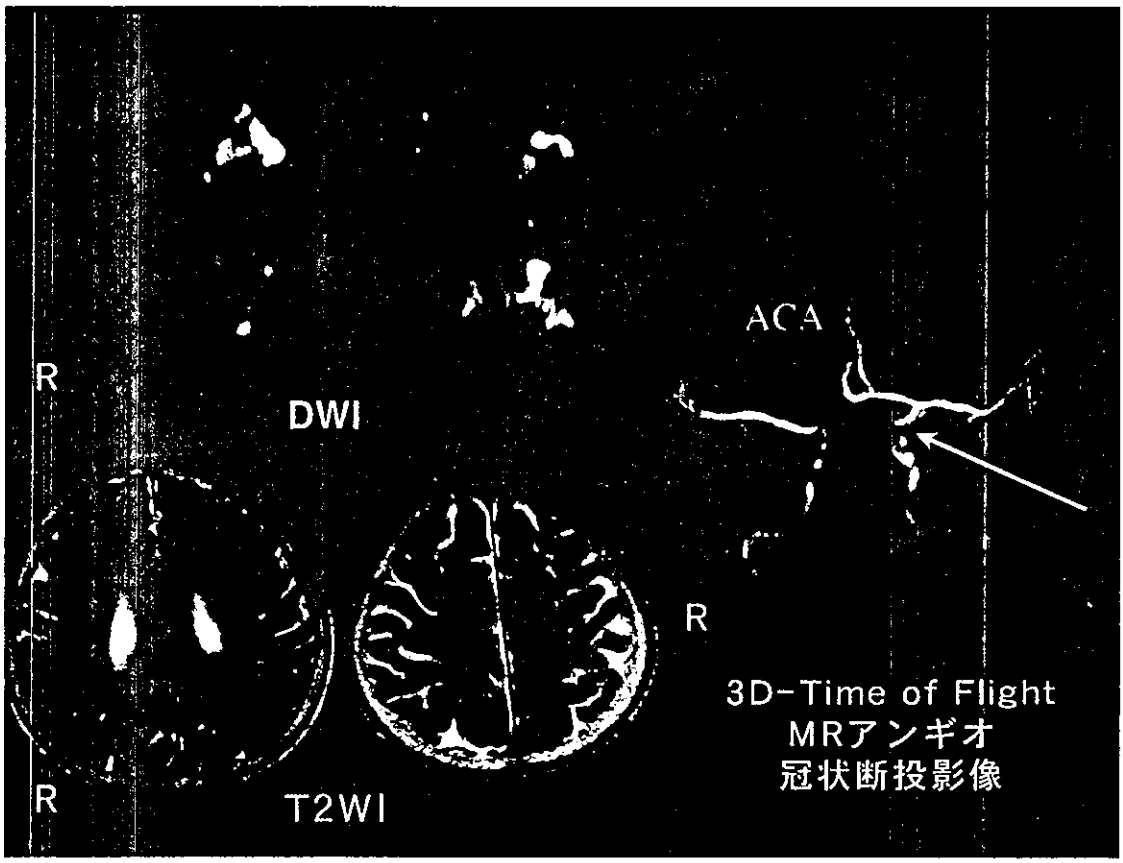

拡散強調画像では，左内頸動脈灌流領域の皮質に多発性に新しい梗塞巣を認める。臨床症状（右片麻痺）で予想されるよりも広汎に右前頭葉内側まで梗塞が広がっているが，MR アンギオでの狭窄病変と右前大脳動脈が左内頸動脈から灌流されている variation から，その病態として左内頸動脈サイフォン部高度狭窄部からの動脈原性塞栓症と診断された。

図　5　　内頸動脈サイフォン部高度狭窄症例

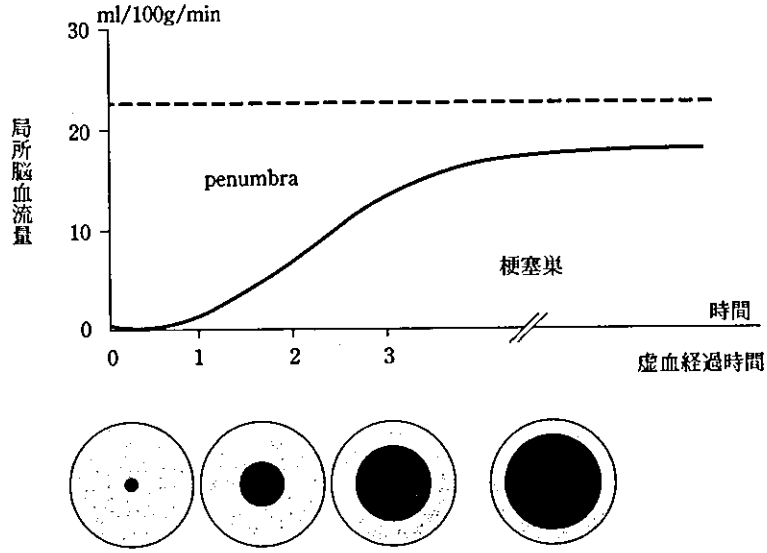

図　6　脳虚血による penumbra と梗塞巣の経時的な変化（中大脳動脈閉塞モデルによる）。Penumbra 領域では時間が経過すると梗塞巣が拡大していく。拡散強調画像では梗塞巣を反映して異常領域は経時的に拡大する。

り巻く虚血領域は，細胞死には至らないものの神経電気活動ができないレベルの虚血である penumbra となっている[8]。この penumbra の概念はもともとの定義が拡大解釈され，最近では，そのままの虚血であると細胞死，つまりは梗塞巣となってしまう領域とも解釈されている。この penumbra は発症当初は拡散強調画像では異常領域として描出することはできない。しかし，この penumbra 領域は，脳循環が再開されないかぎり，時間経過とともに梗塞巣の拡大となり，拡散強調画像を経時的に撮影してみると，徐々に梗塞巣が拡大することになる（図6）。実際，実地臨床でも，撮影時間が早い時期であると，拡散強調画像で予想される領域以上の広い領域の神経脱落症状があり，経時的に拡散強調画像で描出される梗塞巣が拡大していく症例も多い[9]（図7）。

従って，拡散強調画像は梗塞巣の描出には優れているものの，発症直後に撮影された場合の異常高信号領域が最終的な梗塞領域の大きさと一致しない場合が多い点には注意が必要ということになる。

さらに，血栓溶解療法が積極的に行われるようになり，超急性期に拡散強調画像が撮影されるようになると，血栓溶解療法で拡散強調画像の異常高信号領域が小さくなる症例があることが報告されるようになった。それまでは，拡散強調画像の高信号領域は永続的に梗塞になった非可逆性な領域と考えられていたわけであるが，penumbra が拡散強調画像で高信号な領域にも存在する[10]ことが示されたことになる。

V．拡散強調画像と灌流画像の mismatch

このような，penumbra を予測する一つの方法は，灌流画像により脳循環の虚血領域を脳血流低下領域として描出する方法である。これと，拡散強調画像との間に不一致な部分（mismatch）があれば，これが penumbra を示していると考えることができる（図8）。この領域すべてが将来脳梗塞になるとはかぎらないまでも，脳循環を再開させることができれば，この mismatch の領域を助けることができることになる。

逆に，拡散強調画像と灌流画像が一致する場合には，脳梗塞としてかなり完成された状態であることを示しているし，さらに，拡散強調画像の方が広い領域である場合には，途絶していた血流が再開し，luxury perfusion となっていると考えられる。

このように灌流画像を同時にとることと，MR アンギオを同時に行うことで主幹動脈に閉塞があるかどうかを見ることができれば，血栓溶解をはじめとした血流再開治療を早急に行うべきかの治療方針決定に重要な情報を提供できることになる[11]。

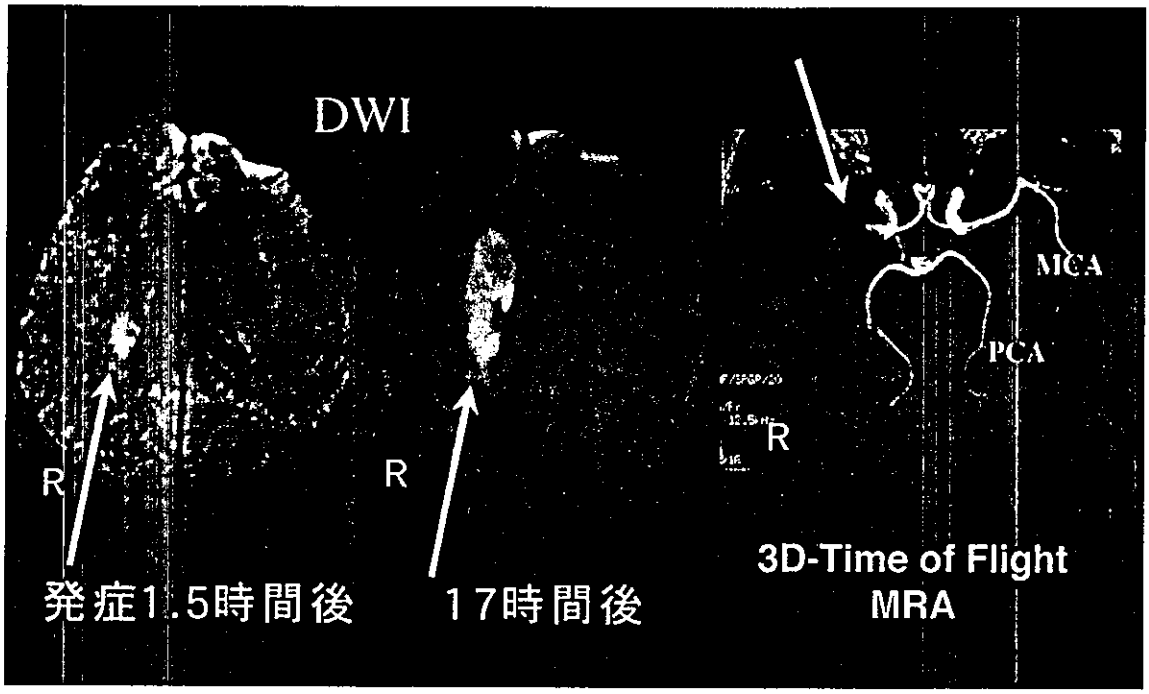

発症1.5時間後にはDWIでは右放線冠に異常を認めるのみであるが，臨床症状は左片麻痺に加えて意識障害と半側無視もあり広汎な虚血が考えられた。MRAにて右中大脳動脈は閉塞し，17時間後にはDWI上，梗塞巣は明らかに拡大していた。

図　7　右中大脳動脈塞栓性閉塞症例

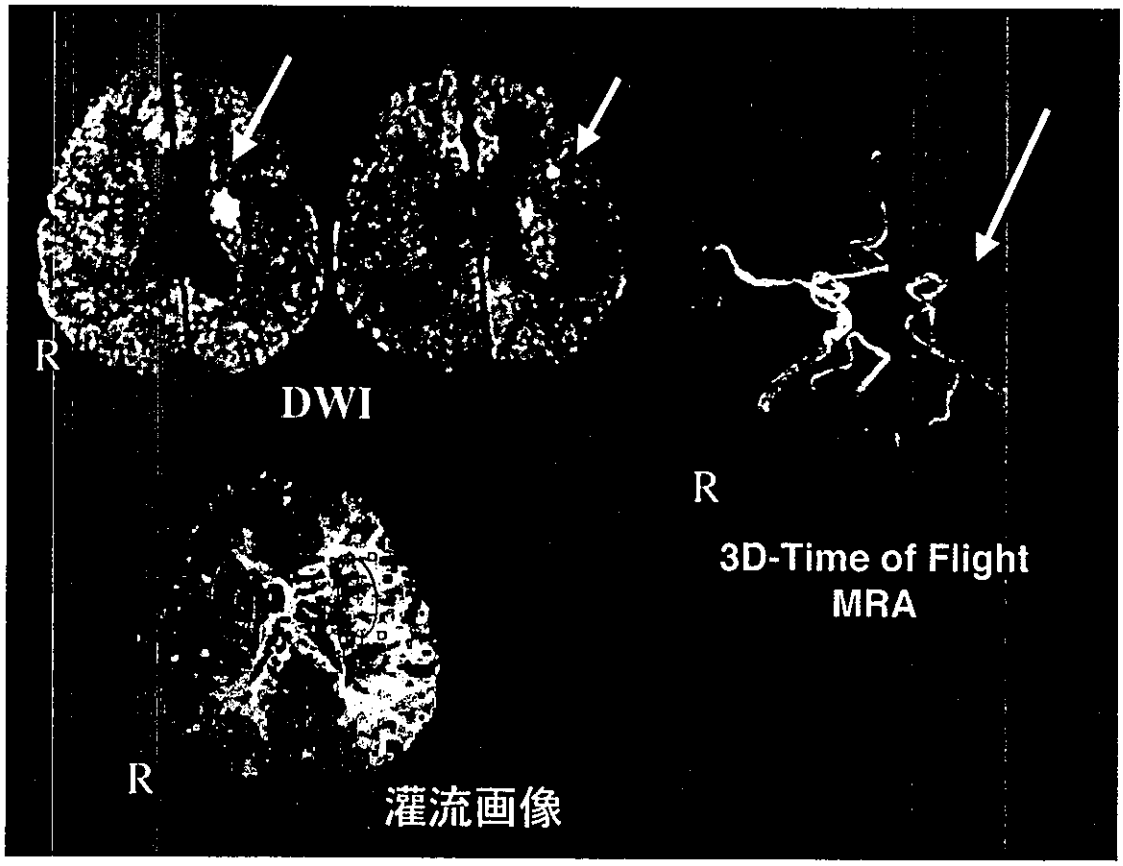

DWIで描出された梗塞巣に比べて灌流画像では左中大脳動脈灌流領域全域の血流低下が認められ，mismatchが存在しており，広汎なpenumbraの存在が示された。

図　8　左中大脳動脈閉塞症例

Ⅵ. Therapeutic Time Window からみた拡散強調画像の意義

血栓溶解薬であるtPAの有用性が1995年米国で発表[12]されて以来，脳梗塞の発症後，できるだけ早い時期に治療を開始すべきであるという超急性期治療が注目されるようになった。NINDSの治験からは，発症3時間以内であればtPAが有用であるが，3時間を超えるとその有用性が認められなくなることから，tPAの経静脈投与による血栓溶解療法のTherapeutic Time Windowは3時間であると考えられている。そこで，このTherapeutic Time Windowからみた拡散強調画像の意義を考えてみたい。

1. 発症3時間以内の脳梗塞

tPAの治験では，24時間いつでも検査できる利便性からCTによる脳出血の除外と，Early CT signが画像上の検討項目となった。経静脈投与による血栓溶解療法ではCTで中大脳動脈の灌流領域の1/3以上に梗塞の所見が認められる場合には，血栓溶解後の予後が不良となる可能性が高いことが報告されている[13]。拡散強調画像を使えば，高信号領域として梗塞巣が明瞭に描出できることから，拡散強調画像で中大脳動脈灌流領域1/3以上の異常を認めるかどうかの診断を容易に行うことができる[6]。また，MRアンギオにより血管閉塞部位の確認が可能であり，さらに灌流画像をとれば，虚血領域と梗塞領域のmismatchもみることができる。これまでの治験では，発症3時間以内であれば血管閉塞と血流検査は行わなくても，脳出血と広汎な脳梗塞が除外できれば，血栓溶解療法は有用であることが報告されている[12]。

2. 発症3～6時間以内の脳梗塞

発症3時間以降の脳梗塞例の中に，血栓溶解をはじめとした血行再開術が有用な症例があるはずであることが指摘されている。中大脳動脈閉塞に限って経動脈性にprourokinaseを用いた血栓溶解療法の有用性が示された[14]ように，症例を選択すれば，血栓溶解療法の適応症例が存在する。実験的な完全虚血モデルとは異なり，臨床では，側副血行や閉塞パターンから，penumbraはかなり長期に渡り存在すること[11]，そのために血行再開することで脳梗塞の進展を押さえられる症例がある可能性が高い。この場合に最もMRの有用性が高いと考えられている。先に述べたごとく，拡散強調画像，灌流画像，MRアンギオを組み合わせれば，閉塞部位と虚血領域と梗塞領域，そのmismatchとしてのpenumbraを描出できる可能性があり，血栓溶解のTherapeutic Time Windowを3時間以上に広げられる可能性がある。そのためにmultimodal MRによる臨床試験が進行中である（DIAS：Desmoteplase in Acute Ischemic Stroke）。

3. 発症6時間以後の脳梗塞

発症6時間を超えると，塞栓性閉塞例でのpenumbraはかなり限られた領域となっている可能性が高い。しかし，血栓性閉塞例では，側副血行の発達が期待できるため，血栓溶解をはじめとした血行再開術の可能性は残っていると思われる。特に椎骨脳底動脈血栓性閉塞に関しては，かなり長いTherapeutic Time Windowを期待できる可能性がある[15]。発症6時間以後でも拡散強調画像と灌流画像のmismatchとMRアンギオによる閉塞部位の確認により，血栓溶解を含めた積極的治療のための適応を決定することができると考えられる。

ま　と　め

拡散強調画像は脳梗塞の超早期における梗塞巣を描出する画像として極めて有用であるが，脳梗塞の臨床病型までにいたる診断においては，これにMRアンギオと灌流画像を組み合わせたMR検査（multimodal MR）が必要である。特に血栓溶解療法における有用性が海外では盛んに検討されているが，早期の的確な臨床病型診断は，血栓溶解薬以外の抗血栓療法の選択や予後の推定，リハビリを含めたADLの拡大の大きな指標となる。しかし，実際の臨床病院においては，MRが緊急検査として行いにくい実態があり，今後，脳卒中のセンター化に伴い24時間稼働可能なMRの必要性がますます増していくものと思われる。

文　献

1) Warach, S., Gaa, J., Siewert, B. et al.: Acute human stroke studied by whole brain echo planar diffusion-weighted magnetic resonance imaging. Ann Neurol, 37: 231-241, 1995.
2) Warach, S., Chien, D., Li, W. et al.: Fast magnetic resonance diffusion-weighted imaging of acute human stroke. Neurology, 42: 1717-1723, 1992.
3) Eastwood, J. D., Engelter, S. T., MacFall, J. F. et al.: Quantitative assessment of the time course of infarct signal intensity on diffusion-weighted images. AJNR Am J Neuroradiol, 24: 680-687, 2003.
4) Burdette, J. H., Elster, A. D., Ricci, P. E.: Acute cerebral infarction: quantification of spin-density and

T2 shine-through phenomena on diffusion-weighted MR images. Radiology, 212: 333-339, 1999.
5) Saur, D., Kucinski, T., Grzyska, U. et al.: Sensitivity and interrater agreement of CT and diffusion-weighted MR imaging in hyperacute stroke. AJNR Am J Neuroradiol, 24: 878-885, 2003.
6) Barber, P. A., Darby, D. G., Desmond, P. M. et al.: Identification of major ischemic change. Diffusion-weighted imaging versus computed tomography. Stroke, 30: 2059-2065, 1999.
7) Koroshetz, W. J., Gonzalez, G.: Diffusion-weighted MRI: an ECG for "brain attack"? Ann Neurol, 41: 565-566, 1997.
8) Astrup, J., Siesjo, B. K., Symon, L.: Thresholds in cerebral ischemia-the ischemic penumbra. Stroke, 12: 723-725, 1981.
9) Baird, A. E., Benfield, A., Schlaug, G. et al.: Enlargement of human cerebral ischemic lesion volumes measured by diffusion-weighted magnetic resonance imaging. Ann Neurol, 41: 581-589, 1997.
10) Barber, P. A., Darby, D. G., Desmond, P. M. et al.: Prediction of stroke outcome with echoplanar perfusion-and diffusion-weighted MRI. Neurology, 51: 418-426, 1998.
11) Parsons, M. W., Barber, P. A., Chalk, J. et al.: Diffusion-and perfusion-weighted MRI response to thrombolysis in stroke. Ann Neurol, 51: 28-37, 2002.
12) Tissue plasminogen activator for acute ischemic stroke. The National Institute of Neurological Disorders and Stroke rt-PA Stroke Study Group. N Engl J Med, 333: 1581-1587, 1995.
13) von Kummer, R., Allen, K. L., Holle, R. et al.: Acute stroke: usefulness of early CT findings before thrombolytic therapy. Radiology, 205: 327-333, 1997.
14) Furlan, A., Higashida, R., Wechsler, L. et al.: Intra-arterial prourokinase for acute ischemic stroke. The PROACT II study: a randomized controlled trial. Prolyse in Acute Cerebral Thromboembolism. Jama, 282: 2003-2011, 1999.
15) Eckert, B., Koch, C., Thomalla, G. et al.: Acute basilar artery occlusion treated with combined intravenous Abciximab and intra-arterial tissue plasminogen activator: report of 3 cases. Stroke, 33: 1424-1427, 2002.

AJNR Am J Neuroradiol 24:1341–1347, August 2003

Heterogeneity of Cerebral Blood Flow in Alzheimer Disease and Vascular Dementia

Takuya Yoshikawa, Kenya Murase, Naohiko Oku, Masao Imaizumi, Masashi Takasawa, Piao Rishu, Yasuyuki Kimura, Yoshitaka Ikejiri, Kazuo Kitagawa, Masatsugu Hori, and Jun Hatazawa

BACKGROUND AND PURPOSE: **Alzheimer disease (AD) and vascular dementia (VaD) are the two major diseases that cause dementia, and early diagnosis is important. Single photon emission CT (SPECT) of cerebral blood flow (CBF) is used for the early detection of dementia and as an auxiliary method for follow-up. AD shows reduced posterior blood flow and VaD manifests reduced anterior blood flow on CBF SPECT images. We examined the usefulness of 3D fractal analysis of CBF SPECT images to objectively quantify the heterogeneity of CBF in patients with AD and VaD.**

METHODS: **Thirty-two patients with AD and 22 with VaD based on neuropsychologic tests and imaging findings, as well as 20 age-matched control subjects underwent technetium-99m hexamethyl propyleneamine oxime CBF SPECT. We then conducted statistical image processing by 3D fractal analysis on reconstructed data. Fractal dimension, an index of heterogeneity, was then calculated for the whole brain, as well as for the anterior and posterior regions of the brain. A higher fractal dimension indicates that the CBF SPECT image is uneven. The ratio of fractal dimension of the anterior region to fractal dimension of the posterior region (A/P ratio) was calculated. Heterogeneity of CBF was compared among the AD, VaD, and control groups.**

RESULTS: **Fractal dimensions of the AD, VaD, and control groups were 1.072 ± 0.179 (mean ± SD), 1.005 ± 0.156, and 0.806 ± 0.06, respectively. A significant difference of fractal dimension was noted between the control group and the two types of dementia ($P < .0001$); however, no significant difference was noted between the AD and VaD groups. The A/P ratios of the AD and VaD groups were significantly different (0.952 and 1.163, respectively; $P < .01$).**

CONCLUSION: **Analysis of CBF SPECT images quantitatively showed that the fractal dimension was significantly higher (indicating heterogeneity) in patients with AD and VaD when compared with age-matched control subjects. Comparison of the A/P ratio on CBF SPECT images between AD and VaD groups showed that the heterogeneity of CBF was posterior-dominant for AD and anterior-dominant for VaD. Thus, 3D fractal analysis enabled a simple and objective evaluation of the heterogeneity of CBF in patients with AD and VaD.**

Determination of the pathology of dementia and the guidelines for treatment is a very important issue because of the aging of our society. Alzheimer disease (AD) and vascular dementia (VaD) are the two major causes of dementia.

Positron emission tomography (PET) or single photon emission CT (SPECT) of cerebral blood flow (CBF) has been used by many authors to examine differences in the dynamics of cerebral circulation and metabolism between AD and VaD (1, 2). A study on the dynamics of cerebral circulation and metabolism in AD showed that reduced blood flow in the temporoparietal association area is common from the early stage before cerebral atrophy is noticeable (3–6). As dementia progresses, blood flow starts to decrease in the frontal lobe (7), while blood flow is relatively well preserved in the pons, primary motor cortex, primary visual cortex of the occipital lobe, basal ganglia, and thalamus. Studies on the relationship between reduced blood flow and pathologic changes of the posterior cortical association area (ranging from the temporal lobe to the parietal lobe) have also been reported (8). Measurement of glucose

Received January 3, 2003; accepted after revision March 14.

From the Departments of Internal Medicine and Therapeutics (T.Y., N.O., M.T., P.R., Y.K., K.K., M.H.), Allied Health Sciences (K.M.), Nuclear Medicine and Tracer Kinetics (M.I., J.H.), and Clinical Neuroscience (Y.I.), Osaka University Graduate School of Medicine, Suita City, Osaka, Japan.

Address reprint requests to Takuya Yoshikawa, MD, Department of Internal Medicine and Therapeutics, Osaka University Graduate School of Medicine (A8), 2–2, Yamadaoka, Suita City, Osaka, 565-0871, Japan; e-mail: yoshi@tracer.med.osaka-u.ac.jp

metabolism in the brain by means of PET has reportedly shown that glucose metabolism is decreased in the posterior cingulate gyrus before any other site in the very early stage of AD (9). There have also been many reports on the dynamics of the cerebral circulation and metabolism in VaD. According to one report on Binswanger disease, which is a clinical variant of VaD, PET has shown that CBF and the cerebral metabolic rate for oxygen are decreased in the white matter as well as in the cortex (10). In addition, a diffuse decrease of CBF was observed at SPECT (11), and reduced blood flow was also commonly seen in the frontal lobe (12, 13). In VaD, abnormalities tend to be detected with cognitive function tests that include parameters for evaluation of frontal lobe function (14). Namely, AD tends to present with posterior-predominant rather than anterior-predominant blood flow reduction, whereas VaD tends to conversely present with anterior-predominant rather than posterior-predominant blood flow reduction.

Although visual evaluation of normal tomograms is the primary method currently used for SPECT in the area of general clinical testing, this method lacks objectivity because it is heavily influenced by differences in image quality and the image display method, as well as by the judgment of the interpreter. It is difficult to establish a region of interest (ROI) in exactly the same location for all subjects in semiquantitative analysis methods that employ the ROI, which are frequently used for nuclear medicine as more objective indexes, because of differences in brain morphology. In addition, the territory of the ROI is limited, but evaluation of locations other than the ROI is impossible, and a subjective influence cannot be avoided during establishment of the ROI. Recent statistical methods for the analysis of functional images have allowed changes that were missed with conventional ROI analysis to be more easily detected. CBF can now be evaluated three-dimensionally by using 3D stereotactic surface projections (15) for the diagnosis of disease that involves dementia. One of the advantages of evaluation by statistical image analysis of 3D sterotactic surface projections is that sites of abnormal CBF and metabolism can be detected more objectively, since correction can be done for anatomic differences among patients, and patient data can be statistically compared with a normal data base on a voxel-by-voxel basis. In this study, we quantified the heterogeneity of CBF, separately from the blood flow distribution, by performing 3D fractal analysis of CBF SPECT images. The fractal dimension calculated by means of 3D fractal analysis was used as an objective index of the heterogeneity of CBF.

The heterogeneity of the distribution of a tracer can provide us with useful information on the functional status of organs and tissues. Fractal analysis is a mathematic tool for dealing with complex systems that have no characteristic length scale (scale invariant) (16). Scale-invariant systems are usually characterized by noninteger dimensions, which are termed fractal dimensions. Fractal geometry allows structures to be quantitatively characterized in geometric terms, even if their forms are irregular and fragmented, because it deals with the geometry of hierarchies and random processes. In this study, fractal analysis was used to assess the heterogeneity of SPECT images. This type of analysis is most useful for characterizing branching structures, such as the pulmonary airways and blood vessels (17, 18). Spatial changes of regional blood flow and metabolism in living organs are measurable by using fractal analysis with PET and SPECT (16, 19–20). The observed variance increases along with the number of subregions studied in an organ (16), and such resolution-dependent variance can be described with fractal analysis (16, 20–21). Biologic systems show considerable spatial and temporal heterogeneity, such as CBF, myocardial blood flow, and pulmonary blood flow (21–23). VaD due to small-vessel disease is fairly common and is hard to distinguish from AD (24, 25). In this study, we examined the use of 3D fractal analysis for objective evaluation of the heterogeneity of CBF in patients with AD or with VaD due to small-vessel disease.

Characteristics of the AD, VaD, and Control groups

Variable Characteristic	AD	VaD	Control
No. of patients	32	22	20
M/F	15/17	12/10	9/11
Age, y*	67.0 ± 10.3	71.2 ± 8.2	67.6 ± 11.3
MMSE score*	19.1 ± 5.8	23.6 ± 3.4	28.5 ± 1.2

* Data are the mean ± SD.

Methods

Subjects

The subjects consisted of 32 patients (15 men, 17 women) with AD (AD group), 22 patients (12 men, 10 women) with VaD (VaD group), and 20 age-matched controls (nine men, 11 women) (control group). The clinical characteristics of these three groups are shown in the Table . All of the subjects were right-handed. CBF SPECT was performed from June 2000 to June 2002. The National Institute of Neurologic and Communicative Disorders and Stroke–Alzheimer Disease and Related Disorders Association, or NINCDS-ADRDA, diagnostic criteria (26) were used to diagnose probable AD. A diagnosis of VaD was made in a comprehensive manner based on the diagnostic criteria proposed by the National Institute of Neurologic Disorders and Stroke–Association International pour la Recherse et l'Enseignement en Neuroscience (NINDS-AIREN) (27), and the criteria for subcortical VaD proposed by Erkinjuntti et al (28). The 22 patients with VaD were classified as having small-vessel disease based on head MR images that revealed small infarcts ranging from 3 to 15 mm in diameter (seen as low signal intensity on T1-weighted images and as high signal intensity on T2-weighted images) in the basal ganglia, thalamus, pons, and deep white matter. The control group consisted of 20 age-matched individuals who attended our outpatient clinic for investigation of headache or dizziness and underwent CBF SPECT, but who had no neuropsychiatric abnormalities and no abnormalities at CT or MR imaging. The Mini-Mental State Examination (MMSE) (29) was performed within 3 months of CBF SPECT for evaluation of cognitive function. Patients who could not undergo the intellectual function test because of conditions such as aphasia were excluded. Informed consent was obtained from all of the subjects and

from family members when a subject could not fully understand the details of the study.

Data Acquisition

Technetium-99m hexamethyl propyleneamine oxime (^{99m}Tc-HMPAO) was created by reconstituting HMPAO with 20 mCi (740 MBq) of fresh ^{99m}Tc pertechnetate. ^{99m}Tc-HMPAO was injected intravenously while the subject rested supine on the scanning bed with the eyes closed in a quiet examination room. SPECT scanning was performed with a four-headed gamma camera (Gamma View SPECT 2000H; Hitachi Medical Corp., Tokyo, Japan), by using a low-energy thin-section parallel-hole collimator (30). The in-plane and axial resolution after reconstruction was 10.0 mm in full-width at half-maximum. SPECT acquisition was performed at 8 seconds per step, with 128 collections over 360°, and data were recorded in a 64 × 64 matrix.

The raw SPECT data were transferred to a nuclear medicine computer (HARP 3; Hitachi Medical Corp.). The projection data were prefiltered with a Butterworth filter (cutoff frequency 0.20 cycles/pixel, order 10) and reconstructed into transaxial sections of 4.0-mm-thick images in planes parallel to the orbitomeatal line. Chang's attenuation correction was applied to the reconstructed data by using an attenuation coefficient of 0.08 cm $^{-}$.

Anatomic Standardization

Anatomic standardization involves fitting individual brains of different sizes and shapes into the configuration of a standard brain with a fixed coordinate system. We used Neurologic Statistical Image Analysis Software (NEUROSTAT) developed by Minoshima et al (15) at the University of Washington to perform anatomic standardization of our SPECT data. First, the midsagittal plane was determined, and the brain angle was corrected for x plane, y plane, and z plane, since the original images obtained with SPECT are angled depending on the position at the time of imaging. Next, the anterior commissure–posterior commissure line, which is the reference line, was fixed based on four reference points (the polus frontalis, the base of the anterior aspect of the corpus callosum, the base of the thalamus, and the polus occipitalis) within the dimension and was matched to the standard brain coordinate system of Talairach and Tournoux (31). Then, linear transformation and nonlinear transformation were performed, and the brain surface was fitted to the contours of the standard brain by deformation. Since NEUROSTAT performs conversion three-dimensionally along the nerve fibers, atrophic brains could also be appropriately converted to the standard brain (32).

Three-Dimensional Fractal Analysis

In fractal geometry, the relationship between a measure (M) and the scale (a) is expressed as follows:

$$M(a) = k \cdot a^{-D}, \quad (1)$$

where k is a scaling constant and D is called the fractal dimension (17). As Equation 1 implies, the quantity $M(a)$ to be measured is a function of the ruler scale and can be a nonconstant. D is one parameter that is useful for this purpose in characterizing organizationally complex structures (33).

CBF SPECT was performed by using ^{99m}Tc-HMPAO, and the cutoff value for the maximal voxel radioactivity on reconstructed images was established by dividing it from 35% to 50% at 11 equal intervals. The number of voxels with radioactivity equal to or above the established cutoff values was calculated. The cutoff value of the maximal radioactivity was defined as a and the total number of voxels measured was defined as $M(a)$, as shown in Equation 1. The cutoff values were changed in sequential order as this process was repeated, and the number of voxels with radioactivity equal to or above the established cutoff values was calculated. Then, the relationship between the number of voxels with a radioactivity equal to or greater than the established cutoff values and each cutoff value was determined. Finally, the relationship between the number of voxels and the cutoff values was converted into natural logarithms and plotted as a linear relationship. The logarithmic cutoff values were plotted on the horizontal axis of a graph, and the logarithmic value of the number of voxels was plotted on the vertical axis. The slope of this line corresponded to the fractal dimension (Fig 1). A higher fractal dimension indicates that the CBF SPECT image is uneven. As shown in Figure 1, one representative CBF SPECT image each was selected from the AD group, the VaD group, and the control group, after which 3D fractal analysis was performed and the fractal dimension was calculated. The fractal dimensions for the AD case, the VaD case, and the control case were 1.320, 1.112, and 0.767, respectively.

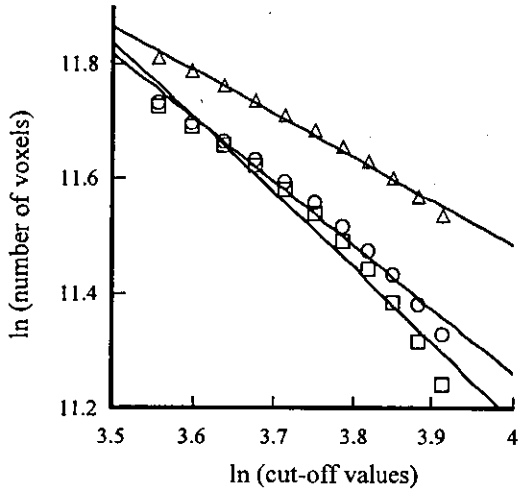

FIG 1. Method for calculating the fractal dimension in one representative case each from the AD group, the VaD group, and the control group. □ indicates AD patient ($y = -1.32x + 16.46$; $r = 0.994$); ○ indicates VaD patient ($y = -1.112x + 15.71$; $r = 0.992$); △ indicates age-matched control ($y = -0.767x + 14.55$; $r = 0.996$)

Items Examined

The fractal dimension of the whole brain was compared among the AD, VaD, and control groups. To examine the differences in CBF between the AD and VaD groups, the cerebrum was divided into anterior and posterior regions by a line connecting the central sulcus on the left and right sides, and the fractal dimension of each region was calculated. The borderline between the anterior region and the posterior region was determined by performing anatomic standardization so that the location did not vary from case to case. The ratio of fractal dimension of the anterior region to fractal dimension of the posterior region was calculated as an anterior-posterior ratio (A/P ratio) and was compared between the AD group and the VaD group.

Statistical Analysis

For comparison of the fractal dimension among the AD, VaD, and control groups, statistical analysis was performed by using the Mann-Whitney U test. The significance of differences in the clinical characteristics of these three groups was assessed with the Mann-Whitney U test. Statistical analysis was performed with the Wilcoxon signed rank test for comparison of the fractal dimension after the data for the AD group and the

FIG 2. A representative case from each group (same cases as in Fig 1). Upper images are T2-weighted MR images; lower images are SPECT images.

A, A 69-year-old woman with AD. T2-weighted MR image does not show any clear abnormality. SPECT image shows blood flow reduction in the bilateral temporoparietal lobes.

B, A 67-year-old man with VaD. Multiple small infarcts are observed in the bilateral basal ganglia on the T2-weighted MR image. A frontal region decrease of CBF is noted on the SPECT image.

C, A 70-year-old female age-matched control subject.

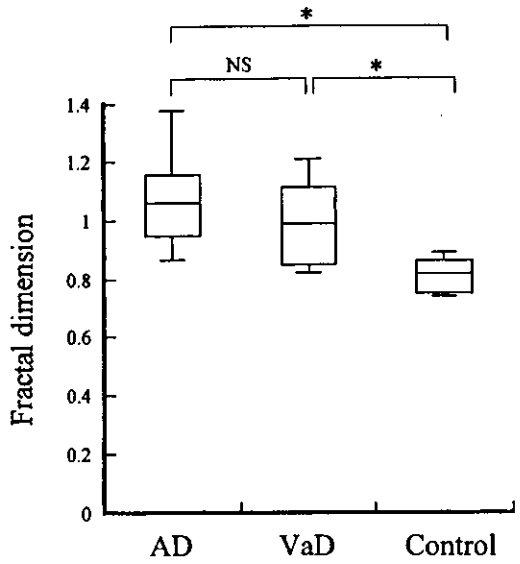

FIG 3. Comparison of fractal dimensions among the AD, VaD, and control groups. Statistical analysis by the Mann-Whitney *U* test showed significant differences (*$P < .0001$) between the control group and the AD group, as well as between the control group and the VaD group. However, no significant difference (*NS*) was noted between the AD group and the VaD group

VaD group were divided into anterior and posterior regions. Results are expressed as mean ± standard deviation (SD), and statistical significance was defined as a P value less than .01.

Results

There were no marked differences in age or sex among the three groups. The MMSE score of the AD group was 19.1 ± 5.8 (mean ± SD), which was lower compared with 23.6 ± 3.4 in the VaD group (Table). However, the result showed no significant difference.

T2-weighted MR images and SPECT images of a representative patient from each group are shown in Figure 2. Although the AD group did not show any clear abnormalities on the T2-weighted MR images, a decrease of CBF in the bilateral temporoparietal lobes was noted on SPECT images. In the VaD group, multiple small infarcts were observed in the bilateral basal ganglia on the T2-weighted MR images, and a frontal region decrease of CBF was noted on SPECT images. The representative cases in Figure 2 are the same as those displayed in Figure 1.

The fractal dimensions in the AD, VaD, and control groups were 1.072 ± 0.179 (mean ± SD), 1.005 ± 0.156, and 0.806 ± 0.06, respectively (Fig 3). The fractal dimension of the whole brain showed a statistically significant difference between the control group and the two groups with dementia ($P < .0001$). In contrast, no significant difference was noted between the AD and VaD groups. The whole brain was divided into anterior and posterior regions, and the fractal dimensions of each region were calculated for comparison between the AD group and the VaD group (Fig 4). In the AD group, the fractal dimension was significantly higher in the posterior region than in the anterior region ($P < .01$), which suggested the presence of posterior-predominant heterogeneity of CBF. In contrast, the VaD group showed a significantly higher fractal dimension in the anterior region than in the posterior region ($P < .01$), which suggested the presence of anterior-predominant heterogeneity of CBF. The A/P ratios of the AD group and the VaD group were 0.952 and 1.163, respectively.

Next, the A/P ratios and fractial dimension of the whole brain were plotted on the horizontal axis and vertical axis, respectively, and each patient in the AD group and the VaD group was examined (Fig 5). A horizontal line was drawn where the mean fractal dimension of the whole brain in the control group was 0.806, and a vertical line was drawn where the A/P ratio was 1 (ie, when the heterogeneity of the anterior region and the posterior region was comparable). Although there was some spread of the data, most points were above the above-mentioned horizontal line in both the AD group and the VaD group. In addition, the two diseases tended to be separated by the A/P ratio of 1, since the AD group tended to have a ratio of 1 or less, whereas the VaD group had a ratio of 1 or more.

Discussion

CBF SPECT may not have much diagnostic significance for VaD compared with degenerative dementia, since VaD is diagnosed with MR imaging in most cases. Although a decrease of CBF and metabolism is naturally observed at sites of infarcts and hemorrhage sites in VaD, a decrease of CBF and metabolism in the cortex that is not limited to such locations can also be seen in diaschisis, and this is why CBF SPECT might have some significance. In a CT study, Loeb et al (34) found no difference in the location or size of

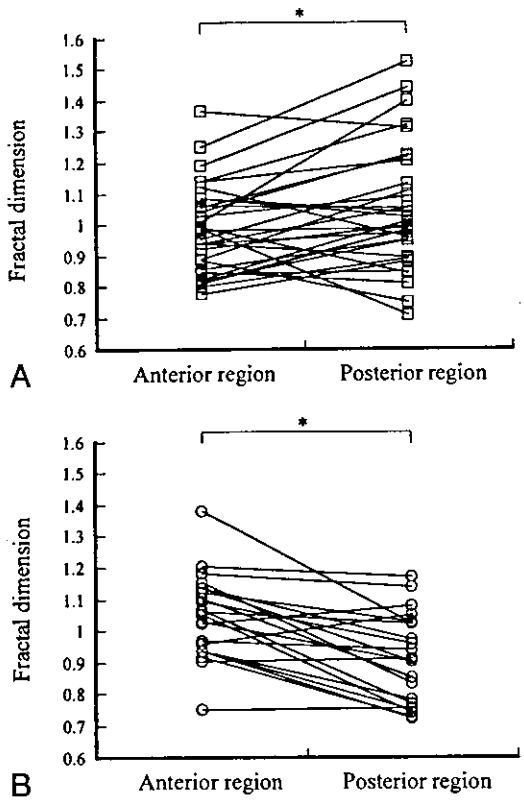

FIG 4. *A*, Fractal dimensions in the AD group plotted for the anterior region and the posterior region. Statistical analysis with the Wilcoxon signed rank test showed that the fractal dimension was significantly greater (*$P < .01$) in the posterior region than the anterior region in the AD group. A/P ratio = 0.952.

B, Fractal dimensions in the VaD group plotted for the anterior region and the posterior region. Statistical analysis with the Wilcoxon signed rank test showed that the fractal dimension was significantly greater (*$P < .01$) in the anterior region than the posterior region in the VaD group. A/P ratio = 1.163

infarcts between a group with dementia and a group without dementia, and they concluded that the morphologic findings on images should be evaluated cautiously. The properties, locations, and clinical features of brain lesions that cause VaD vary markedly from case to case. Therefore, when clinical studies are performed, results may not necessarily be uniform whatever diagnostic criteria are used. For the VaD group in this study, we selected patients with subcortical ischemia, which is relatively common and difficult to differentiate from AD by visual evaluation (24, 25). The primary brain lesions in this pathologic condition are lacunar infarcts due to the small-vessel disease and ischemic white matter lesions. The criteria for subcortical VaD proposed by Erkinjuntti et al (28) were used as the diagnostic criteria. These criteria were established by correcting the subcortical section of the NINDS-AIREN diagnostic criteria for VaD. The reason why blood flow reduction was observed in VaD due to small-vessel disease, even in the cortex where there were no morphologic abnormalities, seemed to be because cerebral circulation and metabolism were decreased as a secondary effect due to disconnection between the deep cerebrum and the cortex (35).

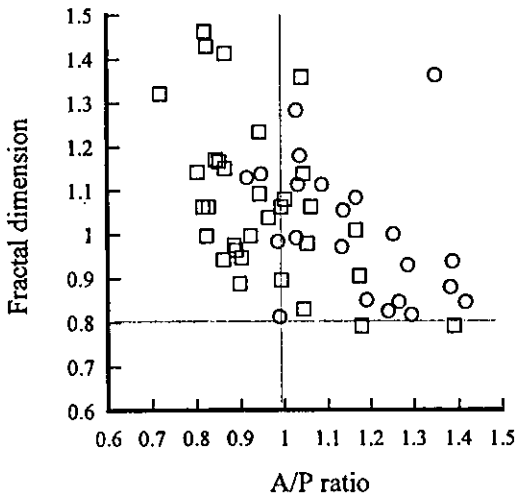

FIG 5. Relationship between the fractal dimension and the A/P ratio in the AD group and the VaD group. Horizontal line is mean fractal dimension of 0.806 for the control group; vertical line is A/P ratio of 1. Examination of individual cases of AD and VaD showed that these diseases tended to be separated by an A/P ratio of 1. □ indicates AD patients (n = 32); O, VaD patients (n = 22)

We performed 3D fractal analysius in the AD, VaD, and control groups and compared fractal dimensions for the whole brain. Our results quantitatively showed that there was heterogeneity of CBF in the AD group and the VaD group compared with the control group, whereas there was no quantitative difference in the heterogeneity of CBF between the AD group and the VaD group. When the whole brain was divided into an anterior region and a posterior region in these two groups and the fractal dimensions were calculated for each region, there was posterior-predominant heterogeneity of CBF in the AD group and there was anterior-predominant heterogeneity of CBF in the VaD group. This is a quantitative confirmation of previous reports suggesting that there is posterior-predominant blood flow reduction in AD versus anterior-predominant blood flow reduction in VaD (1, 2). However, we must be careful, as the fractal dimension is an index of the heterogeneity of CBF and not an index of the extent of blood flow reduction. For example, if blood flow and metabolism are maintained and the CBF distribution is uneven on normal visual evaluation, the fractal dimension will be high even if there is no reduction of blood flow.

In the AD group, some patients had higher fractal dimensions in the anterior region than in the posterior region when individual cases were examined. Since reduced anterior blood flow is also seen in frontotemporal dementia (36), care must be taken to differentiate between these diseases. Although the data are not presented here particularly, the A/P ratio for six cases of frontotemporal dementia was 1.482 ± 0.201(mean ± SD) and was much higher than the A/P ratio for VaD, suggesting the presence of anterior-predominant rather than posterior-predominant heterogeneity of CBF. Some patients with a frontal lobe–predominant reduction on PET scans and who receive a clinical diagnosis of AD may receive a di-

agnosis of frontotemporal dementia several years later. Blood flow reduction in the frontal lobe due to physiologic aging may also be a problem. The VaD group also had patients with a higher fractal dimension in the posterior region than in the anterior region. Since there are also mixed types of AD, it is not rare for AD to be associated with cerebrovascular disease. Examination of autopsy cases has shown that 35–39% of patients with AD also had brain infarction (37). Diagnosis of dementia at the level of MMSE score 20–25 is relatively difficult. The line separating deterioration of cognitive function due to so-called physiologic aging (age-related cognitive impairment) from mild cognitive impairment, which is thought to be a transitional stage toward early dementia, and the line separating mild cognitive impairment from dementia are still unclear (38, 39). Three-dimensional fractal analysis has limited the clinical application owing to the significant overlap in the fractal dimension and the A/P ratio by using fractal analysis in the AD group and the VaD group.

In this study, we performed 3D fractal analysis of CBF SPECT images to quantify the heterogeneity of CBF. Compared with SPECT, PET has superior sensitivity and resolution. Since images obtained by means of fluorine-18–2-fluoro-2-deoxy-D-glucose (^{18}F-FDG) have a better resolution than images obtained by using ^{15}O gas and $H_2{}^{15}O$, this method is widely used for investigation of AD. When correlation of the fractal dimension calculated from CBF SPECT images and ^{18}F-FDG PET images was examined before 3D fractal analysis was applied to CBF SPECT images, there was a significant correlation among the fractal dimensions obtained from each type of image, suggesting that heterogeneity of accumulation on CBF SPECT images was comparable to that on ^{18}F-FDG PET images (40, 41). On the basis of such findings, it seemed that the fractal dimension obtained with CBF SPECT might also reflect CBF and metabolism, and that SPECT can be used instead of PET at institutions that do not have a PET apparatus.

Kuikka et al (16, 42) calculated the fractal dimension as a measure of heterogeneity from the relationship between the relative dispersion (ie, the SD divided by the mean count) and the number of subregions. Although they determined the subregions semiautomatically, this does not appear to be a straightforward method, especially in 3D analysis. However, the 3D fractal analysis method is simple to perform in a 3D manner, does not need special software, and is objective. The most important factor in calculating the fractal dimension from SPECT images is the cutoff value. In this study, the cutoff value for the maximum radioactivity was set at 11 levels from 35% to 50% at equal intervals, and the number of voxels with radioactivity exceeding the cutoff value was calculated in each case. In all cases, the relationship between the cutoff value and the number of voxels (converted to a natural logarithm) was linear, and the correlation coefficient between them was 0.99, which suggested that the CBF SPECT image appeared to have a fractal form for this range of cutoff values and that the cutoff values used in this analysis were reasonable.

Since the shape of the brain varies from patient to patient, it is difficult to divide the brain into an anterior region and a posterior region at the same site in all cases. Also, there is a serious issue of how to divide the brain into an anterior region and a posterior region. Although the central sulcus might have been more accurately identified by placing a thin-section MR image with its extensive anatomic information over a CBF SPECT image, it has now become possible to solve this problem by standardizing the brain shape through conversion of a patient's SPECT images into the standard brain coordinate system of Talairach and Tournoux (31), after which the brain is divided into an anterior region and a posterior region at the line connecting the right and left central sulcus, which is easy to identify anatomically. Recently, statistical imaging has been used to assist in the diagnosis of dementia. Anatomic standardization is performed during this process. Since a common problem for statistical image analysis is the morphologic changes of a patient's brain, particularly the effects of cerebral atrophy, this must be taken into consideration. Because statistical methods can easily detect systemic differences of images, such as those due to imaging equipment and imaging conditions, unity of imaging methods is important.

Conclusion

The 3D fractal analysis method of statistical image analysis allows heterogeneity of CBF in AD and VaD to be quantified and may also allow a simpler and more objective evaluation.

Acknowledgments

We thank Messrs. Yukio Nakamura, Hiroaki Matsuzawa, Kouichi Fujino and Miss Tomoko Fukunaga for helping us to perform the nuclear medicine examinations and for evaluating cognitive function.

References

1. Frackowiak RS, Pozzilli C, Legg NJ, et al. **Regional cerebral oxygen supply and utilization in dementia: a clinical and physiological study with oxygen-15 and positron tomography.** *Brain* 1981;104: 753–778
2. Mielke R, Pietrzyk U, Jacobs A, et al. **HMPAO SPECT and FDG PET in Alzheimer disease and vascular dementia: comparison of perfusion and metabolic pattern.** *Eur J Nucl Med* 1994;21:1052–1060
3. Foster NL, Chase TN, Fedio P, et al. **Alzheimer disease: focal cortical changes shown by positron emission tomography.** *Neurology* 1983;33:961–965
4. Haxby JV, Gray CL, Koss E, et al. **Longitudinal study of cerebral metabolic asymmetries and associated neuropsychological patterns in early dementia of the Alzheimer type.** *Arch Neurol* 1990; 47:753–760
5. Jagust WJ, Friedland RP, Budinger TF, et al. **Longitudinal studies of regional cerebral metabolism in Alzheimer disease.** *Neurology* 1988;38:909–912
6. Holman BL, Johnson KA, Gerada B, et al. **The scintigraphic appearance of Alzheimer disease: a prospective study using technetium-99m-HMPAO SPECT.** *J Nucl Med* 1992;33:181–185

7. Ishii K, Sasaki M, Kitagaki H, et al. **Reduction of cerebellar glucose metabolism in advanced Alzheimer disease.** *J Nucl Med* 1997;38: 925–928
8. Bonte FJ, Weiner MF, Bigio EH, et al. **Brain blood flow in the dementias: SPECT with histopathologic correlation in 54 patients.** *Radiology* 1997;202:793–797
9. Minoshima S, Giordani B, Berent S, Frey KA, Foster NL, Kuhl DE. **Metabolic reduction in the posterior cingulate cortex in very early Alzheimer disease.** *Ann Neurol* 1997;42:85–94
10. Yao H, Sadoshima S, Kuwabara Y, Ichiya Y, Fujishima M. **Cerebral blood flow and oxygen metabolism in patients with vascular dementia of the Binswanger type.** *Stroke* 1990;21:1694–1699
11. Deutsch G, Tweedy JR. **Cerebral blood flow in severity-matched Alzheimer and multi-infarct patients.** *Neurology* 1987;37:431–438
12. Jagust WJ, Bundinger TF, Reed BR. **The diagnosis of dementia with single photon emission computed tomography.** *Arch Neurol* 1987;44:258–262
13. Starkstein SE, Sabe L, Vazquez S, et al. **Neuropsychological, psychiatric, and cerebral blood flow findings in vascular dementia and Alzheimer disease.** *Stroke* 1996;27:408–414
14. Wolfe N, Linn R, Babikian VL, Knoefel JE, Albert ML. **Frontal systems impairment following multiple lacunar infarcts.** *Arch Neurol* 1990;47:129–132
15. Minoshima S, Frey KA, Koeppe RA, Foster NL, Kuhl DE. **A diagnostic approach in Alzheimer disease using three-dimensional stereotactic surface projections of fluorine-18-FDG PET.** *J Nucl Med* 1995;36:1238–1248
16. Kuikka JT, Tiihonen J, Karhu J, et al. **Fractal analysis of striatal dopamine re-uptake sites.** *Eur J Nucl Med* 1997;24:1085–1090
17. Mandelbrot BB. *Fractal geometry of nature.* San Francisco: W. H. Freeman and Company; 1982:131–137
18. Weibel ER. **Fractal geometry: a design principle for living organisms.** *Am J Physiol* 1991;261:361–369
19. Kuikka JT, Bassingthwaighte JB, Henrich MM, Feinendegen LE. **Mathematical modeling in nuclear medicine.** *Eur J Nucl Med* 1991; 18:351–362
20. Kuikka JT, Yang J, Karhu J, et al. **Imaging the structure of the striatum: a fractal approach to SPECT image interpretation.** *Physiol Meas* 1998;19:367–374
21. Bassingthwaighte JB, King RB, Roger SA. **Fractal nature of regional myocardial blood flow heterogeneity.** *Circ Res* 1989;65:578–590
22. Barman SA, McCloud LL, Catravas JD, Ehrhart IC. **Measurement of pulmonary blood flow by fractal analysis of flow heterogeneity in isolated canine lungs.** *J Appl Physiol* 1996;81:2039–2045
23. Nagao M, Murase K, Kikuchi T, et al. **Fractal analysis of cerebral blood flow distribution in Alzheimer disease.** *J Nucl Med* 2001;42: 1446–1450
24. Tatemichi TK, Desmond DW, Paik M, et al. **Clinical determinants of dementia related to stroke.** *Ann Neurol* 1993;33:568–575
25. Meyer JS, Xu G, Thornby J, Chowdhury MH, Quach M. **Is mild cognitive impairment prodromal for vascular dementia like Alzheimer disease?** *Stroke* 2002;33:1981–1985
26. McKhann G, Drachman D, Folstein M, et al. **Clinical diagnosis of Alzheimer disease: report of the NINCDS-ADRDA Work Group under the auspices of Department of Health and Human Services Task Force on Alzheimer disease.** *Neurology* 1984;34:939–944
27. Roman GC, Tatemichi TK, Erkinjuntti T, et al. **Vascular dementia: diagnostic criteria for research studies: report of the NINDS-AIREN International Workshop.** *Neurology* 1993;43:250–260
28. Erkinjuntti T, Inzitari D, Pantoni L, et al. **Research criteria for subcortical vascular dementia in clinical trials.** *J Neural Transm Suppl* 2000;59:23–30
29. Folstein MF, Folstein SE, McHugh PR. **"Mini-mental state": a practical method for grading the cognitive state of patients for the clinician.** *J Psychiatr Res* 1975;12:189–198
30. Kimura K, Hashikawa K, Etani H, et al. **A new apparatus for brain imaging: four-head rotating gamma camera single photon emission computed tomograph.** *J Nucl Med* 1990;31:603–609
31. Talairach J, Tournoux P: **Co-planar stereotaxic atlas of the human brain, three-dimensional proportional system: an approach to cerebral imaging.** New York: translated by Rayport M. Thieme Medical Publishers, Inc.; 1988
32. Minoshima S, Koeppe RA, Frey KA, et al. **Anatomic standardization: linear scaling and nonlinear warping of functional brain images.** *J Nucl Med* 1994;35:1528–1537
33. Nelson T. **Fractal physiologic complexity, scaling, and opportunities for imaging.** *Invest Radiol* 1990;25:1140–1148
34. Loeb C, Gandolfo C, Croce R, Conti M. **Dementia associated with lacunar infarction.** *Stroke* 1992;23:1225–1229
35. Hatazawa J, Shimoscgawa E, Satoh T, Toyoshima H, Okudera T. **Subcortical hypoperfusion associated with asymptomatic white matter lesions on magnetic resonance imaging.** *Stroke* 1997;28: 1944–1947
36. The Lund and Manchester Groups. **Clinical and neuropathological criteria for frontotemporal dementia.** *J Neurol Neurosurg Psychiatry* 1994;57:416–418
37. Snowdon DA, Greiner LH, Mortimer JA, et al. **Brain infarction and the clinical expression of Alzheimer disease: the nun study.** *JAMA* 1997;277:813–817
38. Ritchie K, Touchon J. **Mild cognitive impairment:conceptual basis and current nosological status.** *Lancet* 2000;355:225–228
39. Kogure D, Matsuda H, Ohnishi T, et al. **Longitudinal evaluation of early Alzheimer disease using brain perfusion SPECT.** *J Nucl Med* 2000;41:1155–1162
40. Herhoz K, Schopphoff H, Schmidt M, et al. **Direct comparison of spatially normalized PET and SPECT scans in Alzheimer disease.** *J Nucl Med* 2002;43:21–26
41. Yoshikawa T, Murase K, Oku N, et al. **Statistical image analysis of cerebral blood flow in vascular dementia with small vessel disease.** *J Nucl Med* 2003;44:505–511
42. Kuikka JT, Hartikainen P. **Heterogeneity of cerebral blood flow: a fractal approach.** *Nuklearmedizin* 2000;39:37–42

Mechanical compression of the extracranial vertebral artery during neck rotation

M. Sakaguchi, MD; K. Kitagawa, MD; H. Hougaku, MD; H. Hashimoto, MD; Y. Nagai, MD; H. Yamagami, MD; T. Ohtsuki, MD; N. Oku, MD; K. Hashikawa, MD; K. Matsushita, MD; M. Matsumoto, MD; and M. Hori, MD

Abstract—Using duplex ultrasonography (US), the authors showed compression of the extracranial vertebral artery (ECVA) during neck rotation in 5.0% of 1,108 patients. Age (per 10-year increase, OR 0.80, 95% CI 0.67 to 0.96), vessel diameters (per 0.5-mm diameter increase, OR 0.63, 95% CI 0.51 to 0.79), and symptoms upon neck rotation (OR 4.01, 95% CI 1.35 to 11.9) were associated with vessel compression. In one case, SPECT revealed decreased cerebral perfusion of the hindbrain during rotation. ECVA US is useful in identifying vessel compression, especially in patients with symptoms on neck rotation.

NEUROLOGY 2003;61:845–847

The atlas loop segment of the extracranial vertebral artery (ECVA) is susceptible to mechanical compression during neck rotation toward the contralateral side.[1] ECVA compression can cause hindbrain ischemia and may result in vessel injury.[1-3] We used duplex ultrasonography (US) to investigate the prevalence of and factors associated with ECVA compression during neck rotation in 1,108 individuals. We also determined the regional distribution of cerebral blood flow (CBF) by SPECT in a patient who had blurred vision during neck rotation. Although several transcranial Doppler sonography (TCD) studies have shown reduced flow velocity in the posterior cerebral artery (PCA),[4,5] no information about CBF distribution in such patients has been obtained.

Subjects and methods. *Subjects.* Between 1997 and 2001, 1,335 patients visited our department for neurovascular examination. Patients who provided informed consent (n = 1,324) were evaluated for flow change in the ECVA during neck rotation. Of these patients, 216 were not eligible because of acute-phase stroke (n = 59), dissection of a cervical artery (n = 10) including ECVA stenosis (n = 3), bilateral (n = 2) and unilateral VA occlusion (n = 65), subclavian steal phenomenon (n = 35), severe cervical spondylosis (n = 2), neck tumor (n = 9), severe heart failure (n = 12), or aortic regurgitation with retrograde flow during the diastolic phase (n = 22). Thus, 1,108 patients participated in the study (mean age, 61.4 ± 12.9 years; men/women, 710/398). Clinical manifestations included stroke or TIA (n = 279), ischemic stroke in the posterior circulation (n = 88), Takayasu arteritis (n = 13), ischemic heart disease (n = 299), valvular heart disease (n = 169), arteriosclerosis obliterans (n = 83), aortic aneurysm (n = 118), hypertension (n = 653), diabetes mellitus (n = 309), and hyperlipidemia (n = 433). A total of 136 patients had unexplained vertebrobasilar-distribution symptoms including vertigo (n = 28), dizziness (n = 46), feeling faint (n = 6), loss of consciousness (n = 60), and blurred vision (n = 5). Vessels were excluded when the flow signal was absent or retrograde or when the end-diastolic velocity was zero at a neutral neck position.

Ultrasonographic examination. The longitudinal view of the ECVA was obtained at the C4 to C6 level with a 7.5-MHz linear probe (SSA-260A CE, Toshiba; Tokyo, Japan), and the diameter and flow velocity of the ECVA were measured on both sides.[6,7] Particular care was taken to keep the incident angle between the beam and the vertebral artery at 60 degrees or less, and we calculated the flow velocity after adjustment of the insonation angle. The patient was instructed to rotate the head to the contralateral side with the neck extended and to keep the head in this position for at least 10 seconds. The difference in insonation angles between the two positions was kept less than a few degrees. ECVA compression was diagnosed when end-diastolic velocity declined to zero during rotation.[7]

Statistical analysis. Mean ± SD data are shown. Relations between ECVA compression and predisposing factors were investigated by logistic regression analyses. The $\chi 2$ test was used to analyze differences between five groups defined by age and ECVA diameter.

Results. Most patients showed minimal change in ECVA flow velocity during neck rotation. Zero diastolic flow velocity was observed in 55 individuals (5.0%).

Factors associated with ECVA compression. Of 1,108 patients examined, 136 (12.3%) had unexplained vertebrobasilar-distribution symptoms. The frequency of ECVA compression in these 136 patients (12/136, 9.6%) was significantly higher than that of the remaining 972 patients without vertebrobasilar-distribution symptoms (42/972, 4.3%; $\chi 2 = 6.94$, $p = 0.008$). Symptoms associated with neck rotation occurred in 28 patients during examination (2.3%). All 28 patients had unexplained vertebrobasilar-distribution symptoms. Clinical symptoms during neck rotation include vertigo (n = 9), dizziness (n = 11), feeling faint (n = 4), and blurred vision (n = 4). In two of the four

From the Division of Stroke Research (Drs. Sakaguchi, Kitagawa, Hougaku, Hashimoto, Nagai, Yamagami, Ohtsuki, Matsushita, and Mori), Department of Internal Medicine and Therapeutics (A8), Department of Clinical Neuroscience (Dr. Kitagawa), and Department of Nuclear Medicine (Drs. Oku and Hashikawa), Osaka University Graduate School of Medicine; and Department of Clinical Neuroscience and Therapeutics (Dr. Matsumoto), Hiroshima University Graduate School of Biomedranical Sciences, Japan.

Received July 29, 2002. Accepted in final form May 7, 2003.

Address correspondence and reprint requests to Dr. Kazuo Kitagawa, Division of Stroke Research, Department of Internal Medicine and Therapeutics (A8), Osaka University Graduate School of Medicine, 2-2 Yamadaoka, Suita, Osaka 565-0871, Japan; e-mail: kitagawa@medone.med.osaka-u.ac.jp

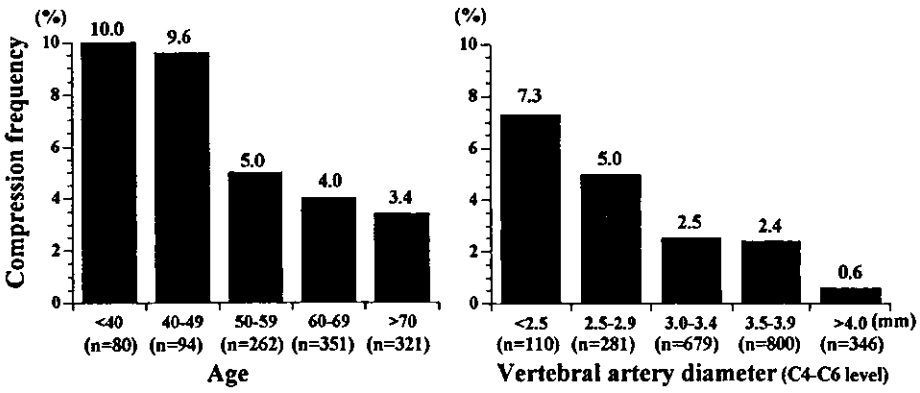

Figure 1. Frequency of extracranial vertebral artery (ECVA) compression by age subgroup (left panel) and in subgroups based on vessel diameter (right panel). Difference among the five age groups was observed (χ^2 = 10.9, p = 0.028). Compression was more frequent in younger age groups (10.0% in those 30 to 39 years of age). Difference among the five diameter groups was observed (χ^2 = 20.6, p = 0.0004). ECVA compression was found more often in narrower vessels.

patients who felt faint and in three of the four with blurred vision, the ECVA was compressed. ECVA compression was not observed in the 20 patients with only vertigo or dizziness during neck rotation. There was no difference in the frequency of ECVA compression between the remaining 108 patients with unexplained vertebrobasilar symptoms (7.4% with ECVA compression) and the 972 patients without unexplained vertebrobasilar symptoms (4.3% with ECVA compression, $\chi 2 = 2.10, p = 0.15$). The frequency of ECVA compression independently decreased with increase in age (figure 1) (OR 0.80, 95% CI 0.67 to 0.96, per 10-year increase), decreased with increasing vessel size (OR 0.63, 95% CI 0.51 to 0.79, per 0.5-mm increase) (see figure 1), and increased with the presence of symptoms on neck rotation (OR 4.01, 95% CI 1.35 to 11.9). There were no relationships between sex, history of stroke, or history of posterior circulation stroke and ECVA compression (table).

Case report. A 56-year-old man who had blurred vision and showed a marked drop in ECVA flow velocity (figure 2, A through C) underwent TCD monitoring of the PCA and angiography, both during neck rotation. SPECT with ^{99m}Tc-hexamethyl propyleneamine oxime (^{99m}Tc-HMPAO) was carried out in the neutral neck position and, 7 days later, during a 2-minute period of submaximal neck rotation. TCD monitoring revealed a marked decline in flow velocity during neck rotation (figure 2D). Angiography showed left VA compression at the C1 to C2 level (figure 2, E and F). In the SPECT study, we found normal distribution of CBF with the neck in the neutral position (figure 2G) but marked decline in CBF in the occipital cortex, cerebellum, and brainstem during submaximal neck rotation (figure 2H).

***Table** Association between factors of interest and risk of extracranial vertebral artery compression during neck rotation in 1,108 subjects*

	Odds ratio (95% CI)	
Factors	Univariate	Multivariate
Age (per 10-y increase)	0.76 (0.63–0.92)*	0.80 (0.67–0.96)†
Sex (men vs women)	1.52 (0.83–2.80)	
ECVA diameter (per 0.5-mm increase)	0.62 (0.50–0.77)‡	0.63 (0.51–0.79)‡
Symptoms during neck rotation	3.36 (1.13–10.1)*	4.01 (1.35–11.9)*
Ischemic stroke	1.23 (0.68–2.24)	
Ischemic stroke in posterior circulation	1.17 (0.45–3.01)	

Odds ratio were analyzed by univariate and multivariate logistic regression with respect to age, symptoms during neck rotation, and extracranial vertebral artery (ECVA) diameter.

* $p < 0.01$.
† $p < 0.05$.
‡ $p < 0.001$.

Discussion. Although ECVA US is simple and highly reproducible, diagnosis of vessel compression may be difficult in cases of VA hypoplasia because a substantial increase in insonation angle may cause diastolic flow to drop below the level of sensitivity. Other studies on the prevalence of VA compression have included small subject numbers.[8] We found that ECVA compression was more frequent in patients with unexplained vertebrobasilar symptoms than in those without such symptoms. Although the numbers were very small, the frequency of ECVA compression was highest in those with faintness or blurred vision associated with neck rotation. In these patients, ECVA compression may cause vertebrobasilar ischemia, as shown in the case presented, and such patients should be treated carefully during neck manipulation, neck exercise, and surgery. However, even in this population, the test was negative in three of eight patients. In these patients, cervical spondylitic compression of the ECVA may be a reason for symptoms because it occurs associated with head turning toward the ipsilateral side, and the spondylitic spurs may be removed at surgery in these cases.[1] Benign paroxysmal postural vertigo can also cause similar symptoms. A rare event of symptomatic ECVA compression is a reflection of collateral blood flow through the contralateral VA or posterior communicating arteries.[3] However, artery compression may promote formation of thrombi that are later propelled intracranially.[9] Although mechanical trauma does not appear to be an important cause underlying vessel dissection,[10] ECVA dissections are observed frequently in the atlas loop segment.[1,2] Although our results provide no evidence that US screening for VA compression should be performed as part of

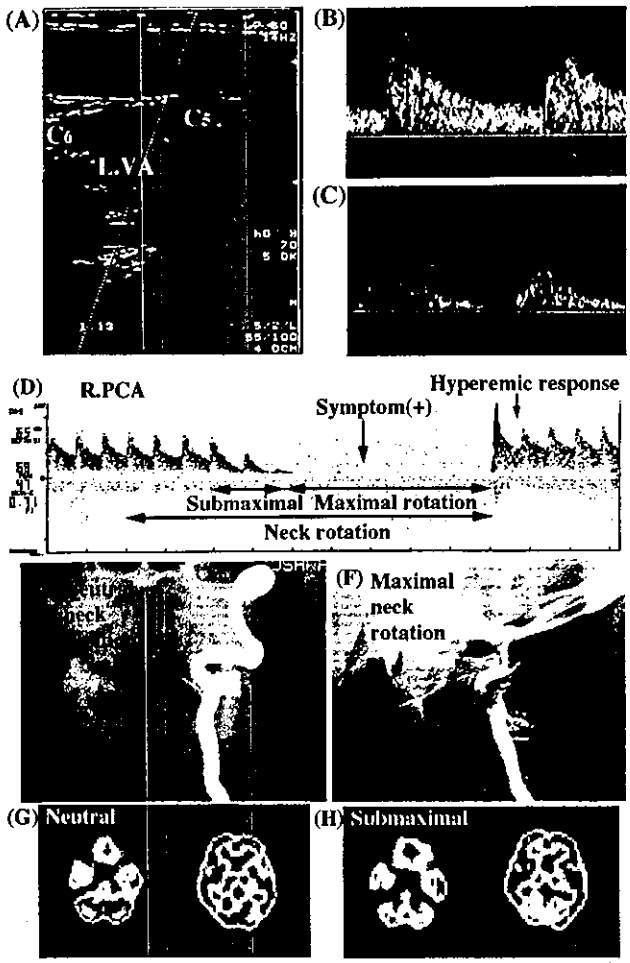

Figure 2. Extracranial vertebral artery (ECVA) compression evaluated with duplex ultrasonography, transcranial Doppler (TCD) monitoring, vertebral angiography, and SPECT findings in a patient with typical vertebrobasilar ischemia. (A) Duplex ultrasonography of left vertebral artery (L.VA) at the C5 to C6 vertebral level with the neck in the neutral position (B) and the maximal rotation position (C) shows marked flow velocity reduction with diastolic component of zero during neck rotation. (D) TCD monitoring of the right posterior cerebral artery (R.PCA) indicates a marked fall in blood flow velocity during maximal neck rotation with blurred vision [Symptom(+)] and a transient increase in blood flow velocity (Hyperemic response) upon returning the head to the neutral position, giving symptom relief. Vertebral angiography obtained with the neck in the neutral position (E) and maximal rotation position (F) shows compression of the artery at the C1 to C2 vertebral level during neck rotation. SPECT at neutral neck position (G) and at submaximal neck rotation without symptoms (H) showed a normal distribution of cerebral blood flow (CBF) at the neutral position but a marked fall in CBF in the cerebellum and occipital cortex during neck rotation.

routine testing, it could be useful in identifying vessel compression, especially in patients with faintness or blurred vision associated with head turning.

References

1. Amarenco P, Caplan LR, Pessin MS. Vertebrobasilar occlusion disease. In: Barnett HJM, Mohr JP, Stein BM, Yatsu FM, eds. Stroke: pathophysiology, diagnosis, and management, 3rd ed. New York: Churchill Livingstone, 1998;513–597.
2. Schievink WI. Spontaneous dissection of the carotid and vertebral arteries. N Engl J Med 2001;344:898–906.
3. Frisoni GB, Anzola GP. Vertebrobasilar ischemia after neck motion. Stroke 1991;22:1452–1460.
4. Brautaset NJ. Provokable bilateral vertebral artery compression diagnosed with transcranial Doppler. Stroke 1992;23:288–291.
5. Sturzenegger M, Newell DW, Douville C, Byrd S, Schoonover K. Dynamic transcranial Doppler assessment of positional vertebrobasilar ischemia. Stroke 1994;25:1776–1783.
6. Bartels E, Flugel KA. Evaluation of extracranial vertebral artery dissection with duplex color-flow imaging. Stroke 1996;27:290–295.
7. Kimura K, Yasaka M, Moriyasu H, Tsuchiya T, Yamaguchi T. Ultrasonographic evaluation of vertebral artery to detect vertebrobasilar axis occlusion. Stroke 1994;25:1006–1009.
8. Jargiello T, Pietura R, Rakowski P, Szczerbo-Trojanowska M, Szajner M, Janczarek M. Power Doppler imaging in the evaluation of extracranial vertebral artery compression in patients with vertebrobasilar insufficiency. Eur J Ultrasound 1998;8:149–155.
9. Tettenborn B, Caplan LR, Sloan MA, et al. Postoperative brainstem and cerebellar infarcts. Neurology 1993;43:471–477.
10. Brandt T, Grond-Ginsbach C. Spontaneous cervical artery dissection. Stroke 2002;33:657–658.

Journal of Neuroscience Research 75:401–407 (2004)

CRE-Mediated Gene Transcription in the Peri-Infarct Area After Focal Cerebral Ischemia in Mice

Shiro Sugiura,[1]* Kazuo Kitagawa,[1] Emi Omura-Matsuoka,[1] Tsutomu Sasaki,[1] Shigeru Tanaka,[1] Yoshiki Yagita,[1] Kohji Matsushita,[1] Daniel R. Storm,[2] and Masatsugu Hori[1]

[1]Division of Strokology, Department of Internal Medicine and Therapeutics, Osaka University Graduate School of Medicine, Suita, Japan

[2]Department of Pharmacology, University of Washington, Seattle

Cyclic AMP response element binding protein (CREB) is a transcription factor expressed constitutively primarily in neurons and is activated by phosphorylation at Ser^{133} residue. CREB mediates expression of several neuroprotective proteins, including B-cell CLL/lymphoma 2 (BCL-2) and brain-derived neurotrophic factor (BDNF). Although phosphorylation of CREB after ischemia has been investigated extensively, CRE-mediated gene transcription after ischemia is not as well studied. We investigated temporal changes in CRE-mediated gene transcription in the cerebral cortex after focal ischemia in transgenic mice with a CRE-lacZ reporter gene. In the ischemic core, X-gal-positive cells, which reflected expression of the CRE-lacZ reporter gene, were observed rarely at any time point, though transient phosphorylation of CREB was detected. In contrast, the peri-infarct area showed a persistent increase in the number of X-gal-positive cells, of which more than half were positive for neuronal nuclei (NeuN). Our results suggest that CRE-mediated gene transcription, the pattern of which is not always consistent with that of CREB phosphorylation, occurs primarily in neurons in the peri-infarct area after focal cerebral ischemia and may be a neuroprotective response against ischemic insult.

Key words: CREB; focal cerebral ischemia; neuroprotection; β-galactosidase; BCL-2

In the central nervous system (CNS) ischemic stress is known to induce various cellular responses, some of which, such as ischemic tolerance, are neuroprotective (Kitagawa et al., 1990; Kirino et al., 1991; Kirino, 2002). It is thought that these adaptive responses are regulated by ischemia-induced genes, the expression of which is triggered largely by several transcription factors. We focused on cyclic AMP response element binding protein (CREB), a transcription factor that is abundant in the brain and particularly in neurons. It is constitutively expressed and activated by phosphorylation at the Ser^{133} residue in response to various extracellular stimuli, including growth factors, neurotransmitters, and ischemic stress. CREB controls expression of several genes that contain a consensus cyclic AMP response element (CRE; TGACGTCA) in the promoter region, including some neuroprotective genes such as BCL-2 (Wilson et al., 1996), and brain-derived neurotrophic factor (BDNF) (Shieh et al., 1998). CREB has been reported to play important roles as a mediator of synaptic plasticity, neuronal growth or survival, and neuroprotection in the developing and mature nervous systems (Ghosh and Greenburg, 1995; Bonni et al., 1999; Riccio et al., 1999; Walton et al., 1999; Finkbeiner et al., 2000; Walton and Dragunow, 2000; Zirpel et al., 2000; Lonze and Ginty, 2002). Our group also revealed that CREB phosphorylation in response to excitotoxic stimuli induced expression of BCL-2 and was involved in the neuroprotective cellular response using CRE-decoy oligonucleotide (Mabuchi et al., 2001). Involvement of CREB phosphorylation in ischemic tolerance has been suggested as well (Mabuchi et al., 2001; Nakajima et al., 2002). Although CREB phosphorylation after ischemia has been investigated extensively (Walton et al., 1996; Hu et al., 1999b; Tanaka et al., 1999, 2001; Mabuchi et al., 2001), to our knowledge CRE-mediated gene transcription after focal ischemia has not been studied. As phosphorylation of CREB at Ser^{133} residue is necessary but not sufficient for activation of CRE-mediated gene transcription (Hu et al., 1999a), the pattern of phosphorylation of CREB may possibly differ from that of CRE-mediated transcription. We examined the pattern of CRE-mediated gene transcription in the

*Correspondence to: Shiro Sugiura, MD, Division of Strokology, Department of Internal Medicine and Therapeutics (A8), Osaka University Graduate School of Medicine, 2-2, Yamadaoka, Suita City, Osaka, 565-0871, Japan. E-mail: siro@medone.med.osaka-u.ac.jp

Received 27 August 2003; Revised 20 October 2003; Accepted 21 October 2003

Published online 18 December 2003 in Wiley InterScience (www.interscience.wiley.com). DOI: 10.1002/jnr.10881